Article

Effects of Anodizing Conditions on Thermal Properties of Al 20XX Alloys for Aircraft

Junghyun Park [1,2], Kyeongsik Son [2], Junghoon Lee [3]🆔, Donghyun Kim [2,*] and Wonsub Chung [1,*]

1   Department of Materials Science and Engineering, Pusan National University, Busan 46241, Korea;
    wythe1007@pusan.ac.kr
2   Korea Institute of Ceramic Engineering and Technology, Gyeongsangnam-dom, Jinju 52851, Korea;
    ksson@kicet.re.kr
3   Department of Metallurgical Engineering, Pukyong National University, Busan 48513, Korea;
    jlee1@pknu.ac.kr
*   Correspondence: dhkim1208@kicet.re.kr (D.K.); wschung1@pusan.ac.kr (W.C.);
    Tel.: +82-55-792-2765 (D.K.); +82-51-510-2386 (W.C.); Fax: +82-55-792-2764 (D.K.); +82-51-510-4457 (W.C.)

Abstract: Anodizing was applied to improve the heat dissipation performance of aluminum (Al) alloys, by forming an oxide layer, such that they could be employed in aerospace applications. The methods employed were hard sulfuric acid (high hardness), soft sulfuric acid (low hardness), boric-sulfuric mixed acid, tin-sulfuric mixed acid, and chromic acid solutions. Each process was completed under optimized conditions. The surface morphology was observed using field emission scanning electron microscopy (FE-SEM) and a digital camera. For the determination of thermal performance, Fourier transform infrared spectroscopy (FT-IR) was used to measure the emissivity at 50 °C, and laser flash analysis (LFA) was utilized to analyze the thermal diffusivity at room temperature to 300 °C. The radiative property of metals is often ignored because of their low emissivity, however, in this research, the emissivity of the metal oxides was found to be higher than that of bare metal series. This study improved the heat dissipation properties by oxidization of Al via the anodizing process.

Keywords: anodizing; thermal diffusivity; heat dissipation; emissivity; aerospace applications

1. Introduction

Aluminum and its alloys exhibit varying properties as a function of the concentration of added trace elements. In particular, the Al 20XX series alloys have high thermal conductivity and workability because of the addition of 2–10 wt.% of copper [1]. Al 20XX alloys can exhibit a higher specific strength and lower specific gravity than those of steel series after age hardening; therefore, they are suitable for fabricating special components for industrial applications [2]. With due to this advantage, aluminum and its alloys are used in up to 80% of the structural materials employed in aircraft components [3,4].

However, aluminum and its alloys have the disadvantage that their strength decrease at high temperature. Generally, the aircraft flies at 800 to 1000 km/h, and the fuselage rise to approximately 100 °C and 200 °C in nose of the aircraft due to friction with the air, which causes structural defects via reduced strength at high temperature [5]. At this point, effective heat dissipation can prevent the high-temperature strength of the surface from decreasing and thus improve the reliability of the aircraft.

To improve heat dissipation, the anodizing process can be applied. The oxide layer formed by anodizing has high thermal radiative properties, which can effectively release heat externally. The radiation energy is expressed as the Stefan–Boltzmann equation, given in Equation (1):

$$E_{radiation} = A \cdot \sigma \cdot \varepsilon \cdot T^4 \tag{1}$$

where $E_{radiation}$ is the radiation energy (W/m^2), and A, T, σ, and ε are the area of the surface (m^2), surface temperature (K), Stefan–Boltzmann coefficient (5.67×10^{-8} W/m^2·K^4),

and emissivity ($0 \leq \varepsilon \leq 1$), respectively. When the surface temperature and emissivity is increased, the radiation performance can be also enhanced [6–9]. Because the temperature of the surface depends on the temperature of the heat source, it is necessary to improve the thermal radiation characteristics by controlling the emissivity. In general, the emissivity is higher in ceramic materials with a black color like as ideal body, as blackbody. By comparison, metallic materials do not have high emissivity because of the high reflectivity. Therefore, aluminum anodizing can improve the thermal radiation properties of the material by forming aluminum oxide on the substrate [6].

Several previous studies reported about anodizing on aluminum for aerospace. However, most of the reports was associated with mechanical properties or corrosion resistance, and the reports about thermal properties were rarely. Besides, most papers on thermal properties for aluminum anodizing have been reported on either thermal conductivity or thermal radiation, and no papers have been found comparing the two heat transfer mechanisms together. Therefore, in this study, thermal conductivity and thermal radiation were considered for aluminum anodizing [10–12].

This study aims to improve the heat dissipation properties of Al 20XX series alloys as a function of anodizing conditions. The electrolytes employed during anodizing were differentiated into hard and soft sulfuric acid, boric-sulfuric mixed acid, tin-sulfuric mixed acid, and chromic acid solutions. Thermal and bonding properties were compared according to the anodizing conditions, and actual heat dissipation was compared using light emitting diode (LED) modules.

2. Materials and Methods

An Al 20XX alloy made of rolled plates, measuring $80 \times 30 \times 2$ mm (length, width, thickness) was used as the substrate. The specimen was immersed in 5.4g/L of Turco 4215 aqueous solution for 8 min at 323 K to obtain a clean, grease-free surface. It was then rinsed with deionized water. After degreasing, the substrate was dipped into 8.2 g/L bonderite solution for 5 min at room temperature to remove the pre-oxide layer.

Table 1 list the anodizing conditions as functions of the anodizing methods; these conditions were optimized via a preliminary experiment [13–16]. After anodizing, the specimens were subjected to the sealing process to fill the pores that were formed by the growth of the anodized layer.

Table 1. The experimental conditions as functions of the kinds of electrolyte for aluminum (Al) anodizing.

	(1)	(2)	(3)	(4)	(5)
	Hard Sulfuric Acid	**Soft Sulfuric Acid**	**Boric-Sulfuric Mixed Acid**	**Tin-Sulfuric Mixed Acid**	**Chromic Acid**
Solution	H_2SO_4 232.5 g/L	H_2SO_4 203.6 g/L	H_2SO_4 45.7 g/L H_3BO_3 8.4 g/L	H_2SO_4 41.3 g/L $C_4H_6O_6$ 82.4 g/L	CrO_3 46.8 g/L
Time	50 min	30 min	25 min	25 min	54 min
Temperature	0–1 °C	21 °C	26 °C	37.5 °C	35 °C
Voltage/Current	3 ASD	17 V	15 V	14 V	45 V

The surface morphology was observed using a field emission scanning electron microscope (FE-SEM, Mira 3, Tescan, Brno, Czech Republic), and the emissivity of the specimens was measured using Fourier transform infrared spectroscopy (FT-IR, M4400-2-2S, MIDAC, Westfield, NJ, USA). The spectral range of the thermal radiation emitted from 5 to 18 μm at 50 °C. In addition, laser flash analysis (LFA, LFA427, NETZCH, Weimar, Germany) was performed to evaluate the thermal diffusivity. The chemical bonding of the surface was analyzed by X-ray photoelectron spectroscopy (XPS, Nexsa, Thermo Fisher Scientific, Waltham, MA, USA) after sputtering etching and the results were calibrated by the C 1s peak. The heat dissipation performance was evaluated using an LED module. The samples were attached to the LED module using silver paste and thermal grease to remove air

pockets. As shown in Figure 1, the temperature of the heatsink and the LED lamp was compared to confirm the heat dissipation performance of the samples.
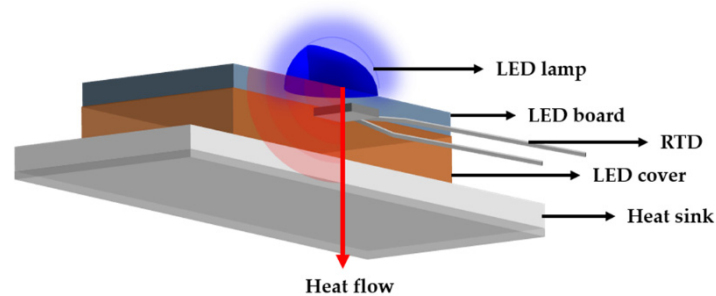
Figure 1. Schematic representation of performance test with a LED module.

3. Results and Discussion

Figure 2 shows the surface morphology of the anodized specimens, determined using FE-SEM. Note that the optical images are included to observe the color of the surfaces in the FE-SEM images. The samples under all conditions can be seen to have a relatively uniform sealing process. In addition, in the case of aluminum anodizing, the color of the surface commonly does not change before and after the anodizing treatment. However, sample (1) demonstrated coloration because of increasing internal defects, such as pores, cracks, and mis-orientations [13].
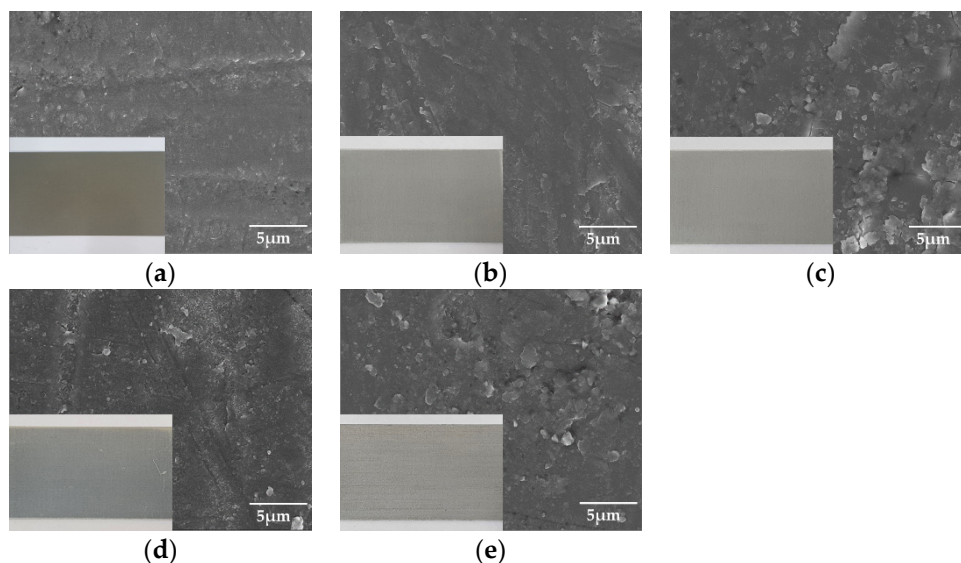
Figure 2. The surface morphologies of anodized surface using field emission scanning electron microscope (FE-SEM) with optical images: (**a**) hard sulfuric acid, (**b**) soft sulfuric acid, (**c**) boric-sulfuric mixed acid, (**d**) tin-sulfuric mixed acid, and (**e**) chromic acid.

Figure 3 shows the binding energy of Al 2p, which indicates the anodized surface by XPS analysis. The analysis was performed for the oxide surface after 400 s sputtering etching, at an estimated Ta_2O_5 (0.04 nm/s) sputter rate, and the spectra were corrected using the C 1s peak (284.8 eV). The peaks at 74.48 and 75.50 eV confirm the presence of Al-O and Al-OH bonds, respectively. Regardless of the conditions of the anodizing process, Al-O bonds were commonly observed on the surface, and the Al-O bonding (74.48 eV) was estimated to be a ceramic such as Al_2O_3 [17,18].
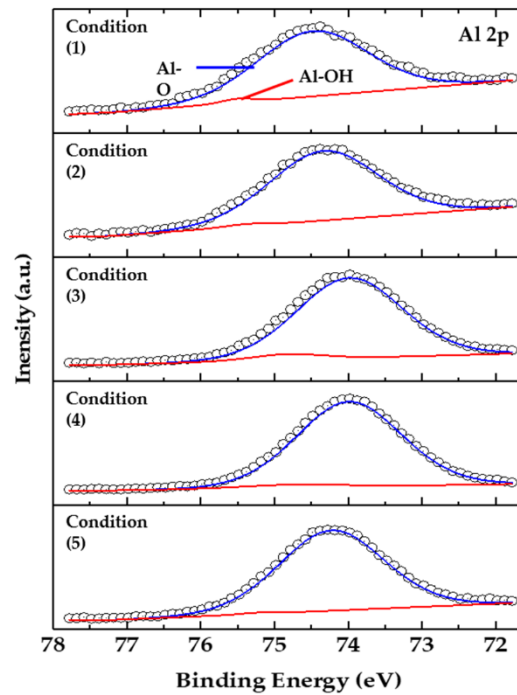
Figure 3. XPS spectra of Al 2p core lever as a function of process conditions (1)–(5).

Figure 4 shows the emissivity of each specimen at 50 °C as a function of anodizing conditions with the bare Al substrate. According to previous research, metallic materials have a very low emissivity of 0.2 or less [19,20], and the emissivity value of bare Al was found to be 0.217, as listed in Table 2. Although the emissivity varied as a function of the anodizing electrolytes, it had a value of 0.900 or more, and was significantly increased with the anodizing treatment. When the hard sulfuric acid and tin-sulfuric acid were applied to the aluminum anodizing, the values of emissivity were the highest 0.936 and 0.930 at 50 °C, respectively. It can be estimated that the difference in emissivity is due to the different fractions of pores produced in the anodizing process. The formed pores provide resistance to heat transfer [21,22]. Because the emissivity of condition (4) is the highest among the conditions (2)–(5), which present the processes in which pores occur, it can be seen to have the lowest fraction of pores. In addition, condition (1) is considered to have high emissivity because it is a process in which pores are not formed.
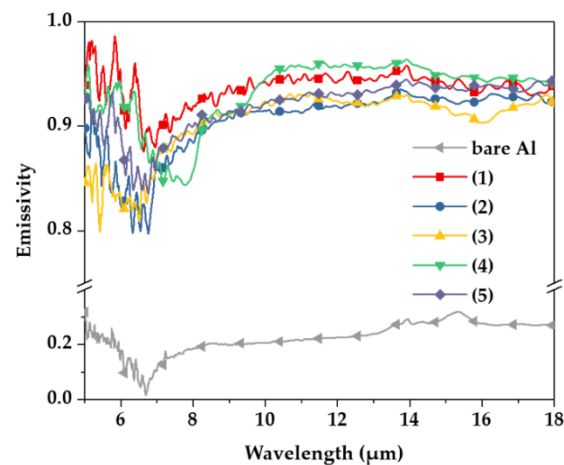

Figure 4. Emissivity of samples measured at wavelengths of 5 to 20 μm using FT-IR spectroscopy.

Table 2. The value of emissivity as a function of anodizing conditions at 50 °C.

|	**Al Substrate**	**(1)**	**(2)**	**(3)**	**(4)**	**(5)**
Emissivity	0.217	0.936	0.904	0.906	0.930	0.918

In addition, thermal diffusivity was examined using laser flash analysis from room temperature to 300 °C, as shown in Figure 5. Because the thermal diffusivity is closely related to the thermal conductivity of the materials, it is common to have a high value in metallic materials, such as bare Al. However, the thermal diffusivity decreases with the increasing temperature because of the increased thermal resistance and reduced binding energy due to the vibration of metal atoms [23]. In addition, because ceramic as oxide materials have a higher binding energy and heat capacity than metallic materials, they have the opposite tendency of metallic materials [24]. If the binding energy and heat capacity are high, a large amount of heat can be removed from the metallic materials, and the heat dissipation effect is maximized. With the exception of condition (1), the thermal diffusivity increases as the temperature increases, close to that of the bare Al. However, the sample of condition (1) had low thermal diffusivity, which can be inferred from an internal defect, which is equivalent to Figure 2a [13].
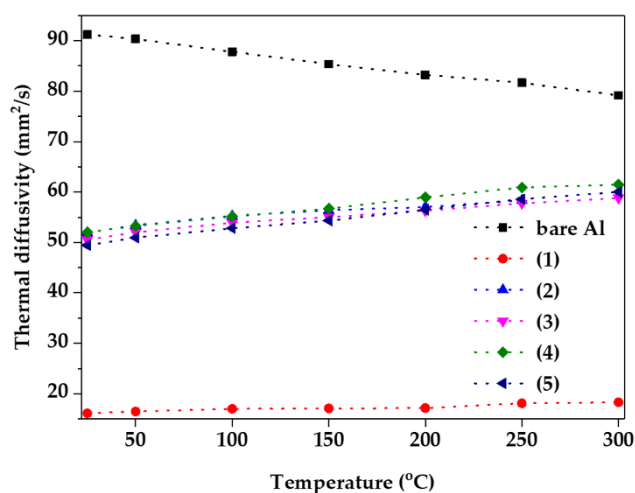
Figure 5. Thermal diffusivity of samples as a function of anodizing condition from room temperature to 300 °C.

In addition, a sealing treatment using Ni and B ions was performed to obtain equivalent results under all conditions, and the concentrations of Ni and B varied depending on the conditions, as shown in Figure 6. This is because the pore morphology of the oxide layer formed by anodizing was different. A closed anodized layer was generated under condition (1), and the sealing electrolyte was not detected by XPS. However, pores were formed and filled by Ni and B ions, in the other conditions. The sample of condition (4) formed a dense oxide layer and condition (2) formed a thin oxide layer.

The results of the hardness test are shown in Figure 7 as a function of anodizing conditions and indicate the density of the oxide layers. The density of the oxide layer can also be determined by the depth of the pressed materials because it was indented with a force that did not affect the substrate. An indenter (a diamond for the Vickers hardness test) was inserted into each sample with equal force, and the hardness was calculated via the size of the indentation on the surface. The specific values are listed in Table 3. When condition (4) was used, the hardness was higher than that in all other conditions. That is, the sample of condition (4) had the highest density oxide layer according to the concentration of Ni and B ions (by XPS) and the hardness test, as shown in Figures 6 and 7, respectively. The oxide layer formed through anodizing has a large number of pores, which

works as a thermal barrier. The pores were filled by the sealing electrolyte, but no wonder it was less robust than the oxide layer formed by chemical bonds with the substrate. The dense oxide layer means that it contains fewer pores and can be concluded that fewer factors are preventing thermal transfer. In layers composed of same components, it can be a reasonable inference that high hardness samples have high thermal transfer properties.
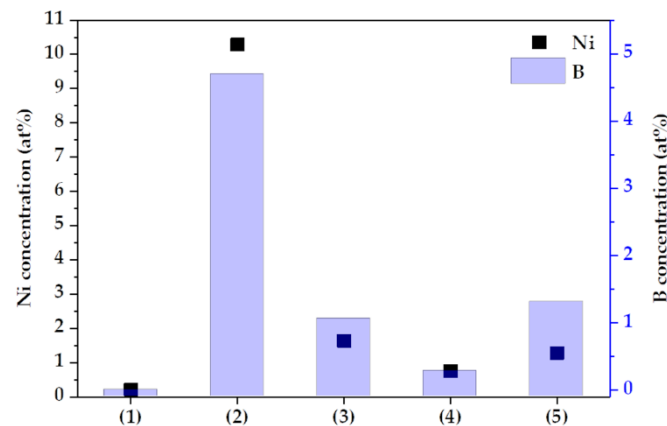
Figure 6. The concentration of Ni and B as a function of anodizing conditions.
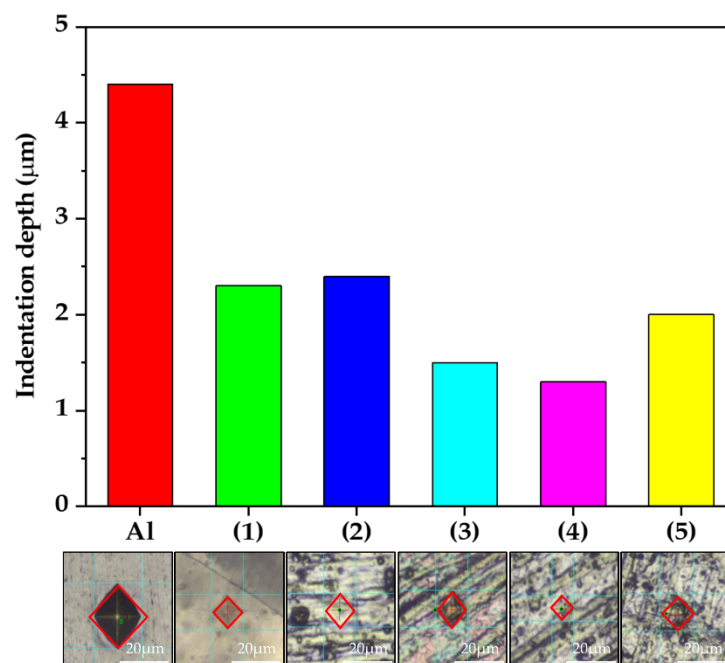

Figure 7. The indentation depth and optical image of the oxidized surface according to the Vickers hardness test (0.01 kg/f).

Table 3. Surface hardness of samples depending on anodizing conditions.

	Al Substrate	(1)	(2)	(3)	(4)	(5)
Hardness (Hv)	50	300	230	370	470	280

Finally, the heat dissipation performance was evaluated via practical application, and the results are shown in Figure 8. An LED module was applied for the test, and the temperature of the RTD and the surface of the heat sink was evaluated, as shown in Figure 1. Figure 8a measured the temperature between LED and heat sink, and Figure 8b

was the temperature of the heat sink surface. Therefore, as more heat was transferred to the outside through the heat sink, the temperature between LED and heat sink decreased and the surface temperature increased. The RTD temperature was measured in real time until the temperature was stabilized for 1400 s. When the tin-sulfuric acid was applied to the heat sink, it had the lowest temperature value compared to the other specimens (Figure 8a), and the surface temperature had the highest value (Figure 8b). These results indicate that the movement of heat from the inside to the outside was faster than that of other LED modules because of the improvement of the heat dissipation performance, suggesting that a large amount of heat was concentrated in the heat sink and dissipated [25,26]. From a long-term perspective, the lifetime of the LED could be extended when using a tin-sulfuric acid heat sink.
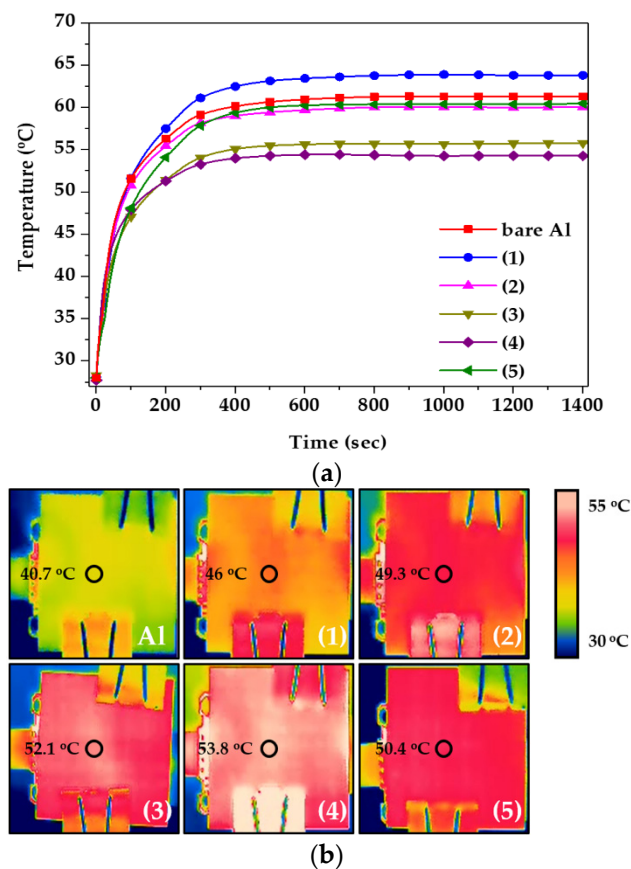
Figure 8. (**a**) Heat dissipation performance and (**b**) surface heat distribution by IR camera, as functions of anodizing conditions.

4. Conclusions

In this work, measured not only thermal diffusivity which is the main factors of thermal conductivity but also emissivity which is the main factor of thermal radiation are depending on the anodizing conditions of Al 20XX alloys, and heat dissipation was compared using actual LED modules. The key points of our study are as follow:

(1) The oxide layer formed on the aluminum substrate by anodizing process reduced thermal diffusivity and increased emissivity.

(2) The oxide layer formed via tin-sulfuric acid solution was confirmed to be the densest by XPS and hardness results with the highest thermal diffusivity and emissivity.

(3) The temperature of LED attached with the specimen formed through the tin-sulfuric acid solution was approximately 10% lower than when the bare aluminum was attached.

(4) That is, the temperature of the aircraft surface would be reduced when formed a dense oxide layer using an appropriate anodizing process on Al 20XX alloys.

References

1. Markopoulos, A.P.; Papazoglou, E.L.; Karmiris-Obratański, P. Experimental study on the influence of machining conditions on the quality of electrical discharge machined surfaces of aluminum alloy Al 5052. *Machines* **2020**, *8*, 12. [CrossRef]
2. Rambabu, P.; Prasad, N.E.; Kutumbarao, V.; Wanhill, R. Aluminium alloys for aerospace applications. *Aerosp. Mater. Mater. Technol.* **2017**, 29–52. [CrossRef]
3. Starke, E., Jr.; Staley, J.T. Application of modern aluminum alloys to aircraft. *PrAeS* **1996**, *32*, 131–172. [CrossRef]
4. Zhang, P.; Li, Y.; Liu, Y.; Zhang, Y.; Liu, J. Analysis of the microhardness, mechanical properties and electrical conductivity of 7055 aluminum alloy. *Vacuum* **2020**, *171*. [CrossRef]
5. Dursun, T.; Soutis, C. Recent developments in advanced aircraft aluminium alloys. *Mater. Des.* **2014**, *56*, 862–871. [CrossRef]
6. Kim, D.; Sung, D.; Lee, J.; Kim, Y.; Chung, W. Composite plasma electrolytic oxidation to improve the thermal radiation performance and corrosion resistance on an Al substrate. *Appl. Surf. Sci.* **2015**, *357*, 1396–1402. [CrossRef]
7. Yao, Z.; Hu, B.; Shen, Q.; Niu, A.; Jiang, Z.; Su, P.; Ju, P. Preparation of black high absorbance and high emissivity thermal control coating on Ti alloy by plasma electrolytic oxidation. *Surf. Coat. Technol.* **2014**, *253*, 166–170. [CrossRef]
8. Ge, Y.; Wang, Y.; Zhang, Y.; Guo, L.; Jia, D.; Ouyang, J.; Zhou, Y. The improved thermal radiation property of SiC doped microarc oxidation ceramic coating formed on niobium metal for metal thermal protective system. *Surf. Coat. Technol.* **2017**, *309*, 880–886. [CrossRef]
9. Zhao, B.; Li, L.; Zhang, K.; Yu, K.; Liu, Y. Study on the changes of emissivity of basic copper carbonate in the decomposition process. *Int. J. Heat Mass. Transf.* **2019**, *139*, 641–647. [CrossRef]
10. Abrahami, S.T.; Kok, J.M.M.; Terryn, H.; Mol, J.M.C. Toward Cr(VI)-free anodization of aluminum alloys for aerospace adhesive bonding applications: A review. *Front. Chem. Sci. Eng.* **2017**, *11*, 465–482. [CrossRef]
11. Shao, L.; Li, H.; Jiang, B.; Liu, C.; Gu, X.; Chen, D. A comparative study of corrosion behavior of hard anodized and micro-arc oxidation coatings on 7050 aluminum alloy. *Metals* **2018**, *8*, 165. [CrossRef]
12. Jayakrishna, K.; Kar, V.R.; Sultan, M.T.; Rajesh, M. 1-Materials selection for aerospace components. *Sustain. Compos. Aerosp. Appl.* **2018**, 1–18. [CrossRef]
13. Lee, J.; Kim, Y.; Jung, U.; Chung, W. Thermal conductivity of anodized aluminum oxide layer: The effect of electrolyte and temperature. *Mater. Chem. Phys.* **2013**, *141*, 680–685. [CrossRef]
14. Lambert, M.; Marotta, E.; Fletcher, L. The thermal contact conductance of hard and soft coat anodized aluminum. *J. Heat Transfer.* **1995**. [CrossRef]
15. Yu, S.; Wang, L.; Wu, C.; Feng, T.; Cheng, Y.; Bu, Z.; Zhu, S. Studies on the corrosion performance of an effective and novel sealing anodic oxide coating. *J. Alloys. Compd.* **2020**, *817*, 153257. [CrossRef]
16. Costenaro, H.; Queiroz, F.M.; Terada, M.; Olivier, M.G.; Costa, I.; De Melo, H.G. Corrosion protection of AA2524-T3 anodized in tartaric-sulfuric acid bath and protected with hybrid sol-gel coating. *Key Eng. Mater.* **2016**, *710*, 210–215. [CrossRef]
17. Lu, W.; Iwasa, Y.; Ou, Y.; Jinno, D.; Kamiyama, S.; Petersen, P.M.; Ou, H. Effective optimization of surface passivation on porous silicon carbide using atomic layer deposited Al_2O_3. *RSC Adv.* **2017**, *7*, 8090–8097. [CrossRef]
18. Batra, N.; Gope, J.; Vandana; Panigrahi, J.; Singh, R.; Singh, P.K. Influence of deposition temperature of thermal ALD deposited Al_2O_3 films on silicon surface passivation. *AIP. Adv.* **2015**, *5*, 067113. [CrossRef]
19. Wen, C.-D.; Mudawar, I. Emissivity characteristics of roughened aluminum alloy surfaces and assessment of multispectral radiation thermometry (MRT) emissivity models. *Int. J. Heat Mass. Transf.* **2004**, *47*, 3591–3605. [CrossRef]
20. Zou, Y.; Wang, Y.; Zhang, H.; Wei, D.; Jin, T.; Wang, H.; Liao, S.; Jia, D.; Zhou, Y. Al_2O_3/reduced graphene oxide double-layer radiative coating for efficient heat dissipation. *Mater. Des.* **2018**, *157*, 130–140. [CrossRef]
21. Lee, J.; Kim, N.; Choi, C.-H.; Chung, W. Nanoporous anodic alumina oxide layer and its sealing for the enhancement of radiative heat dissipation of aluminum alloy. *Nano Energy* **2017**, *31*, 504–513. [CrossRef]
22. Liu, Z.; Sun, Q.; Song, Y.; Wang, H.; Chen, X.; Wang, X.; Jiang, Z. Preparation of Mn doped Al_2O_3 heat-dissipating coatings on titanium alloy by cathodic plasma electrolytic deposition. *Vacuum* **2019**, *159*, 228–234. [CrossRef]

23. Luo, Y.; Yang, X.; Feng, T.; Wang, J.; Ruan, X. Vibrational hierarchy leads to dual-phonon transport in low thermal conductivity crystals. *Nat. Commun.* **2020**, *11*, 1–10. [CrossRef]
24. Ohtaki, M.; Tsubota, T.; Eguchi, K.; Arai, H. High-temperature thermoelectric properties of $(Zn_{1-x} Al_x) O$. *J. Appl. Phys.* **1996**, *79*, 1816–1818. [CrossRef]
25. Kim, D.; Lee, J.; Kim, J.; Choi, C.-H.; Chung, W. Enhancement of heat dissipation of LED module with cupric-oxide composite coating on aluminum-alloy heat sink. *Energy Convers. Manag.* **2015**, *106*, 958–963. [CrossRef]
26. Wang, H.; Qu, J.; Peng, Y.; Sun, Q. Heat transfer performance of a novel tubular oscillating heat pipe with sintered copper particles inside flat-plate evaporator and high-power LED heat sink application. *Energy Convers. Manag.* **2019**, *189*, 215–222. [CrossRef]